


**Magnon transport and thermal properties of confined anisotropic CrI<sub>3</sub>**Hengyi Xu \* and Yang Liu*The School of Physics and Technology, Nanjing Normal University, Nanjing 210023, People's Republic of China*Xiaoming Zhu *Nanjing Institute of Astronomical Optics & Technology, Chinese Academy of Sciences, Nanjing 210042, People's Republic of China*

(Received 6 January 2024; revised 28 February 2024; accepted 6 March 2024; published 19 March 2024)

In this study, we derive the expressions of transmission and reflection for the quasi-one-dimensional spin-wave system in the presence of anomalous quadratic interactions due to the Holstein-Primakoff transformation, which are the generalization of Fisher-Lee formula in electronic systems. We employ the Green's function technique to calculate the coherent transport in nanowires with two terminals by considering the exchange randomness and spin dilution. The quantized magnon transmission is modified by both types of disorder, leading to reduced mean-free paths which could be relevant for the implementation of unconventional logic gates. In the linear response regime, the longitudinal thermal conductance divided by temperature shows a broad peak corresponding to a maximum release of entropy, implying the development of spin-correlations. This behavior resembles that of longitudinal and transverse thermal conductivity revealed in the Kitaev model within the framework of quantum spin liquids. These results provide insights into the mechanisms of magnon transport in quasi-one-dimensional spin-wave systems, paving the way for further research on anisotropic magnets and their potential applications in novel computational devices.

DOI: [10.1103/PhysRevB.109.115425](https://doi.org/10.1103/PhysRevB.109.115425)**I. INTRODUCTION**

Magnons are quantized low-energy collective excitations of the spin waves in ferromagnetic or antiferromagnetic materials, and their manipulation has opened up a new avenue for exploring topological phases in condensed matter, forming an emerging field in spintronics [1–5]. Magnonics is concerned with the transport behaviors of spin waves in the nanometer scale and investigates their abilities to carry and process spin information with excellent coherence and low dissipation [6]. Therefore, the propagation and evolution of magnons in spin systems are central issues in magnonics. Theoretical study has indicated that magnon wave packets may undergo self-rotation [7], and a rotational motion along the sample edges gives rise to the thermal Hall effect which can be measured experimentally [8,9]. The correction to the thermal transport coefficient due to the orbital motions has been taken into account within the framework of the linear response theory [10]. Furthermore, disorder can induce the decoherence of magnons and generate Joule heat, making the investigation of the disorder effects on the magnon transport highly desirable. Nasu *et al.* have studied the transport and thermodynamic properties of two types of disorder in the Kitaev model and revealed two distinct mechanisms of disorder [11]. Within these efforts, the relevant studies in the two-dimensional (2D) structures are also rapidly growing [12–14].

In the research field of 2D materials, one of the most exciting developments is the finding of magnetic orderings

in various compounds and van der Waals heterostructures, such as layered  $A_2\text{IrO}_3$  ( $A = \text{Li}$  or  $\text{Na}$ ) [15–17],  $\alpha\text{-RuCl}_3$  [18–20], as well as the monolayers of  $\text{CrGeTe}_3$  [21] and  $\text{CrI}_3$  [22]. These nanoscale systems offer an ideal platform for studying the interplay between low-dimensional electronic and magnetic phenomena with quantum confinement, for example, the magnetoelectric effect [23,24] and spin-valley polarization [25].

Among these materials, the ferromagnetic  $\text{CrI}_3$  as a layered transition-metal compound is particularly interesting by virtue of its frustrated structure and anisotropic exchange interactions. This exchange anisotropy stabilizes ferromagnetism in the 2D systems, otherwise thermal fluctuations due to finite temperature spoil the magnetic orderings according to the Mermin-Wagner theorem [26,27]. In  $\text{CrI}_3$ , the chromium ions surrounded by six neighboring iodine atoms constitute a honeycomb lattice in which magnons play an important role in determining the magnetic and related thermal properties [28]. The magnon Hall effect has been observed in the ferromagnetic insulator  $\text{Lu}_2\text{V}_3\text{O}_7$  [29] and its theoretical interpretations based on the magnon Berry phases have been proposed [7,30–33]. In an analogous way, the thermal Hall conductivity of  $\text{CrI}_3$  has been investigated theoretically in terms of magnon topology [14]. In most previous studies [34], a 2D geometry of systems is assumed, whereas the quasi-one-dimensional (Q1D)  $\text{CrI}_3$  where one of degree of freedom is confined has not been explored, to the best of our knowledge. In this work, we devote our efforts to studying the magnon transport and thermal properties of Q1D  $\text{CrI}_3$  monolayer based on the generalized Green's function technique for coherent transport in bosonic systems.

\*hengyi.xu@njnu.edu.cn

The purpose of the present paper is twofold. First, we derive the detailed Green's function formalism for spin-wave systems. This approach generalizes the Fisher-Lee relation [35] in electronic systems to the counterpart for bosonic systems in which the anomalous magnon interactions emerge due to the Holstein-Primakoff transformation [36] or Schwinger boson mean-field method [34]. Second, we consider the quantized magnon transport in confined CrI<sub>3</sub> nanowires with magnetic anisotropy. The longitudinal thermal conductance is calculated using the magnon transmission based on the above Green's function method.

The paper is organized as follows: in Sec. II, we formulate our model and develop the theoretical formalism for magnon transport. The calculation results are presented and discussed in Sec. III. Section IV contains the summary and conclusions.

## II. MODEL AND THEORETICAL METHOD

### A. Spin-wave Hamiltonian of CrI<sub>3</sub>

The ferromagnetism of CrI<sub>3</sub> is governed by the honeycomb lattice composed of the chromium ions with a magnetic moment  $S = 3/2$ , and can be described by the Heisenberg-Kitaev Hamiltonian

$$\mathcal{H} = - \sum_{\langle i,j \rangle} (J \mathbf{S}_i \cdot \mathbf{S}_j + K S_i^x S_j^x) - \sum_i A (S_i^z)^2, \quad (1)$$

where the first summation runs over the nearest neighboring spin, in which the first and second terms account for the isotropic Heisenberg exchange with the strength  $J$  and the anisotropic Kitaev contribution with the strength  $K$ , respectively. The magnetic anisotropy is described by three directions of the Cr<sub>2</sub>I<sub>2</sub> plaquettes, viz.,  $\hat{\mathbf{v}}_1 = (0, -\sqrt{2/3}, \frac{1}{\sqrt{3}})$ ,  $\hat{\mathbf{v}}_2 = (\frac{1}{\sqrt{2}}, \frac{1}{\sqrt{6}}, \frac{1}{\sqrt{3}})$ ,  $\hat{\mathbf{v}}_3 = (-\frac{1}{\sqrt{2}}, \frac{1}{\sqrt{6}}, \frac{1}{\sqrt{3}})$ , whereupon  $S_i^z = \mathbf{S}_i \cdot \hat{\mathbf{v}}_i$  [14]. The second summation comes from the easy-axis anisotropy of magnitude  $A$ .

The isotropic and anisotropic exchanges can be written concisely as  $-\sum_{\langle i,j \rangle} \mathcal{J}_{ij} \mathbf{S}_i \cdot \mathbf{S}_j$  with exchange coupling  $\mathcal{J}_{ij}$  depending on the link directions. The three possible links of exchange interactions are expressed uniformly as  $\mathcal{J}_a = J + K \hat{\mathbf{v}}_a \otimes \hat{\mathbf{v}}_a$  with  $a \in \{1, 2, 3\}$  labeling the bond directions. Using the Holstein-Primakoff transformation:

$$\begin{aligned} S_{i,\mu}^x &\simeq \sqrt{S/2} (\gamma_{i,\mu}^\dagger + \gamma_{i,\mu}), \\ S_{i,\mu}^y &\simeq i\sqrt{S/2} (\gamma_{i,\mu}^\dagger - \gamma_{i,\mu}), \\ S_{i,\mu}^z &\simeq S - \gamma_{i,\mu}^\dagger \gamma_{i,\mu}, \end{aligned} \quad (2)$$

with  $i$  being the lattice index and  $\mu \in \{A, B\}$  denoting the type of sites in the unit cell of honeycomb lattices, whereby  $\gamma_{i,A}^\dagger (\gamma_{i,A}) \equiv a_i^\dagger (a_i)$  and  $\gamma_{i,B}^\dagger (\gamma_{i,B}) \equiv b_i^\dagger (b_i)$  represent bosonic creation and annihilation operators for the  $A$  and  $B$  sites, respectively. Substituting Eq. (2) into Eq. (1), we obtain the spin-wave Hamiltonian as

$$\begin{aligned} \mathcal{H}_{\text{spw}} &= \sum_i (3J + K + 2A) S a_i^\dagger a_i + \sum_i \alpha_a (a_i^\dagger b_i + a_i b_i^\dagger) \\ &+ \sum_i (\beta_a a_i^\dagger b_i^\dagger + \beta_a^* a_i b_i), \end{aligned} \quad (3)$$

where the normal quadratic terms stand for the particle-particle couplings with the strength  $\alpha_a = -(\mathcal{J}_a^{xx} + \mathcal{J}_a^{yy})S/2$  in terms of the components of the strength matrix  $\mathcal{J}_a$ . Analogous to the Bogoliubov-de Gennes Hamiltonian for superconductors, Eq. (3) contains the anomalous pairings like  $a_i^\dagger b_i^\dagger$  and  $a_i b_i$  arising from Kitaev anisotropic exchanges with the strength  $\beta_a = -(\mathcal{J}_a^{xx} - \mathcal{J}_a^{yy})S/2 - i\mathcal{J}_a^{xy}S$  ( $i$  is the imaginary unit).

Furthermore, the matrix elements of exchanges along  $\delta_1$  are given by  $\mathcal{J}_1^{xx} = J$ ,  $\mathcal{J}_1^{yy} = J + 2K/3$ ,  $\mathcal{J}_1^{zz} = J + K/3$ , and  $\mathcal{J}_1^{xy} = 0$ . Along the link  $\delta_2$ , we have  $\mathcal{J}_2^{xx} = J + K/2$ ,  $\mathcal{J}_2^{yy} = J + K/6$ ,  $\mathcal{J}_2^{zz} = J + K/3$ ,  $\mathcal{J}_2^{xy} = K/(2\sqrt{3})$ . For the third link along  $\delta_3$ , the values are  $\mathcal{J}_3^{xx} = J + K/2$ ,  $\mathcal{J}_3^{yy} = J + K/6$ ,  $\mathcal{J}_3^{zz} = J + K/3$ ,  $\mathcal{J}_3^{xy} = -K/(2\sqrt{3})$ . The values of  $J$ ,  $K$ , and  $A$  can be obtained from the first-principle calculations [37]. Throughout this work, we adopt  $J = 0.53$  meV,  $K = 4.07$  meV, and  $A = 0.44$  meV [14]. The magnon couplings for normal and anomalous quadratic terms are given by

$$\alpha_1 = \alpha_2 = \alpha_3 = -JS - \frac{K}{3}S, \quad (4)$$

and

$$\begin{aligned} \beta_1 &= \frac{K}{3}S, \\ \beta_{2,3} &= -\frac{K}{6}S \mp i\frac{K}{2\sqrt{3}}S. \end{aligned} \quad (5)$$

The total number of magnons is not conserved due to the presence of anomalous terms of  $a^\dagger b$  or  $ab^\dagger$  in Eq. (3), leading to the failure of the conventional Bogoliubov transformation for diagonalization of Hamiltonians. To this end, the generalized Bogoliubov-Valatin transformation or Colpa's algorithm should be employed. In this approach, the eigenmodes can be obtained by diagonalizing  $\sigma_3 \mathbb{H}_{\text{spw}}$  instead of original Hamiltonian to retain the bosonic commutation relations, where  $\mathbb{H}_{\text{spw}}$  is the matrix form of  $\mathcal{H}_{\text{spw}}$  [38,39].

The eigenmodes from the Colpa's algorithm constitute a paraunitary matrix  $\mathcal{U}$  which satisfies

$$\mathcal{U}^\dagger \sigma_3 \mathcal{U} = \sigma_3, \quad \mathcal{U} \sigma_3 \mathcal{U}^\dagger = \sigma_3, \quad (6)$$

where

$$\sigma_3 = \begin{pmatrix} \mathbb{1}_{N \times N} & 0 \\ 0 & -\mathbb{1}_{N \times N} \end{pmatrix}, \quad (7)$$

where  $\mathbb{1}$  is the unitary matrix with the dimension  $N$  dependent on the system size in real space.

### B. Green's function theory for magnon transport

The eigenproblem of the present spin-wave system can be written as

$$\sigma_3 \mathbb{H}_{\text{spw}} \Psi = \omega \Psi, \quad (8)$$

where  $\omega$  is the eigenfrequency of magnons which are the quanta of spin waves. Here we have set  $\hbar = 1$  for brevity in this section. In this work, we are dealing with the QID systems such that the discrete Hamiltonian of the spin-wave system is decomposed into three parts for computational

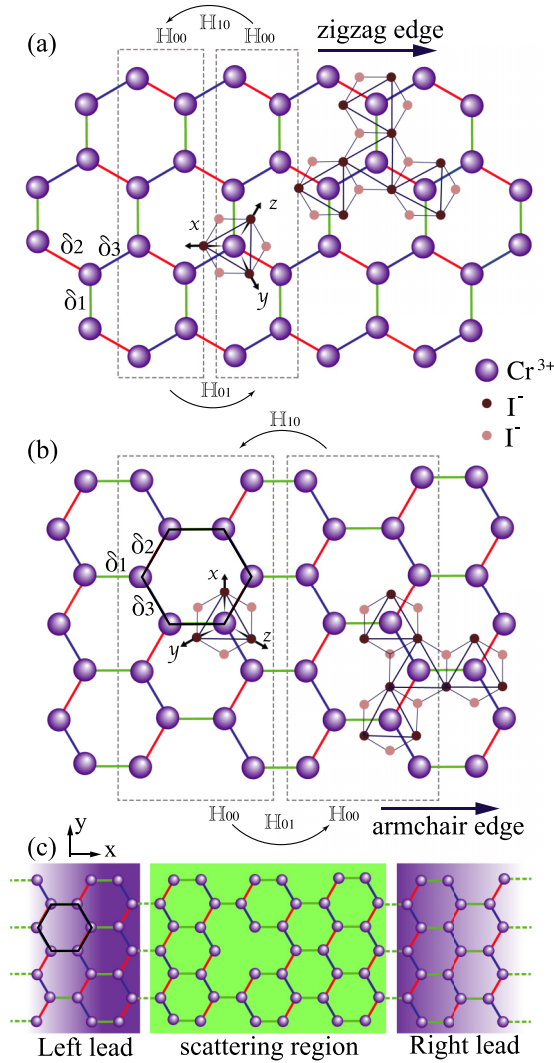


FIG. 1. Schematic of the honeycomb lattice composed of  $\text{Cr}^{3+}$  ions with (a) zigzag and (b) armchair edges. The  $\text{Cr}^{3+}$  ions (violet) lie in an octahedron made up of the upper and lower planes of iodine ions indicated by light (upper) and dark (lower) brown circles.  $x$ ,  $y$ ,  $z$  are the octahedral coordinate axes. The sites boxed by the dashed rectangles represent the unit cells depicted by the Hamiltonian  $\mathbb{H}_{00}$  in our calculations. The couplings between two neighboring unit cells are denoted by  $\mathbb{H}_{01}$  and  $\mathbb{H}_{10}$ . The anisotropic exchanges depend on the three links,  $\delta_1$ ,  $\delta_2$ , and  $\delta_3$ . (c) Schematic setup of the considered two-terminal device with armchair edges along the transport direction.

convenience as

$$\mathbb{H}_{\text{spw}} = \sum_{j=-\infty}^{\infty} \mathbb{H}_{00}|j\rangle\langle j| + \mathbb{H}_{01}|j\rangle\langle j+1| + \mathbb{H}_{10}|j+1\rangle\langle j|, \quad (9)$$

where  $j$  is the index of unit cells in the Q1D system.  $\mathbb{H}_{00}$  is the Hamiltonian of unit cells, and  $\mathbb{H}_{01}$  ( $\mathbb{H}_{10}$ ) represents the forward (backward) coupling between the nearest-neighboring unit cells as shown in Fig. 1. The entire system comprises numerous such unit cells and can be divided into three computational regions, as shown in Fig. 1(c): the central region

where significant scattering occurs, and two semi-infinite leads attached to the scattering region from the left and right. To account for the effects from the leads, we first derive the surface Green's function and the related physical quantities such as the self-energy and linewidth function for magnon transport.

For an infinitely long system, the discrete Schrödinger equation can be written as

$$(\omega - \sigma_3 \mathbb{H}_{00})\mathbf{u} - \lambda^* \sigma_3 \mathbb{H}_{10} \mathbf{u} - \lambda \sigma_3 \mathbb{H}_{01} \mathbf{u} = 0, \quad (10)$$

where  $\lambda = e^{ik}$  with  $k$  being the wave vector of the spin wave. Here the lattice constant is assumed to be 1.  $\mathbf{u}$  is a vector representing the wave function of the unit cell and can be normalized through  $\mathbf{u}^\dagger \sigma_3 \mathbf{u} = \pm 1$  in contrast with the fermion case  $\mathbf{u}^\dagger \mathbf{u} = 1$ . Multiplying both sides of the above equation by  $\lambda$ , we arrive at

$$[(\omega - \sigma_3 \mathbb{H}_{00})\lambda - \lambda^2 \sigma_3 \mathbb{H}_{01}] \mathbf{u} = \sigma_3 \mathbb{H}_{10} \mathbf{u}, \quad (11)$$

which can be recast into a matrix form as

$$\begin{pmatrix} \mathbb{O} & \mathbb{1} \\ -\sigma_3 \mathbb{H}_{10} & \omega - \sigma_3 \mathbb{H}_{00} \end{pmatrix} \begin{pmatrix} \mathbf{u} \\ \lambda \mathbf{u} \end{pmatrix} = \lambda \begin{pmatrix} \mathbb{1} & \mathbb{O} \\ \mathbb{O} & \sigma_3 \mathbb{H}_{01} \end{pmatrix} \begin{pmatrix} \mathbf{u} \\ \lambda \mathbf{u} \end{pmatrix}, \quad (12)$$

where  $\mathbb{O}$  denotes the zero matrix whose size is determined by the number of sites in the unit cell. Solving this generalized eigenproblem, we can obtain the dispersion relations of magnons.

Define the retarded and advanced Green's function for magnons [31,40],

$$\mathcal{G}^{r/a}(\omega) = (\omega - \sigma_3 \mathbb{H}_{\text{spw}} \pm i\eta)^{-1}, \quad (13)$$

where  $\eta$  is an infinitesimal positive number. The local density of states (DOS) for magnons associates with the imaginary part of Green's function

$$\text{DOS}(\omega, \mathbf{r}) = \mp \frac{1}{\pi} \text{Im}[\mathcal{G}^{r/a}(\omega; \mathbf{r}, \mathbf{r})], \quad (14)$$

where  $\text{Im}[\dots]$  takes the imaginary part, and  $\mathcal{G}^{r/a}(\omega; \mathbf{r}, \mathbf{r})$  represents the diagonals of Green's function matrix in real space dependent on the frequency  $\omega$ .  $\mathbf{r}$  denotes the site indices representing a position in real space.

To compute the perturbations recursively, Dyson's equation is extremely useful, which is expressed for magnons as

$$\mathcal{G}^{r/a} = \mathcal{G}_0^{r/a} + \mathcal{G}^{r/a} \sigma_3 \mathbb{V} \mathcal{G}_0^{r/a} = \mathcal{G}_0^{r/a} + \mathcal{G}_0^{r/a} \sigma_3 \mathbb{V} \mathcal{G}^{r/a}, \quad (15)$$

where  $\mathbb{V}$  is a perturbation to the original Hamiltonian.  $\mathcal{G}^{r/a}$  and  $\mathcal{G}_0^{r/a}$  are the Green's functions corresponding to the Hamiltonians with and without perturbations, respectively.

With the definition Eq. (13), we are ready to define the surface Green's function which takes into account the effects of leads. For the right ( $R$ ) lead, it is calculated in virtue of its periodicity as [41]

$$\mathfrak{g}_R^r = (\omega - \sigma_3 \mathbb{H}_{00} - \sigma_3 \mathbb{H}_{01} \mathfrak{g}_R^r \sigma_3 \mathbb{H}_{10})^{-1}. \quad (16)$$

The left-surface Green's function  $\mathfrak{g}_L^r$  can be calculated similarly. Based on the solutions of Eq. (12), the right-surface Green's function can be further expressed as

$$\mathfrak{g}_R^r \sigma_3 \mathbb{H}_{10} = \mathcal{U} \Lambda \mathcal{U}^{-1}, \quad (17)$$

where the matrix  $\mathcal{U}$  consists of the eigenvectors  $\{u\}$  of the right-propagating magnon states with positive group velocities, and the matrix  $\Lambda$  is constructed by placing the corresponding eigenvalue  $\lambda$  on the diagonal.

For the left-propagating states with negative group velocities, we can obtain the left surface Green's function as

$$g_L^r \sigma_3 \mathbb{H}_{01} = \mathcal{U} \Lambda \mathcal{U}^{-1}, \quad (18)$$

where  $\mathcal{U}$  comprises the eigenvectors of the left-propagating states, and the diagonal of  $\Lambda$  contains the corresponding eigenvalue  $\lambda$ .

Define the self-energy of the right lead,

$$\Sigma_R^r = \mathbb{H}_{01} g_R^r \sigma_3 \mathbb{H}_{10}, \quad (19)$$

and its Hermitian conjugate

$$\Sigma_R^a = (\Sigma_R^r)^\dagger = \mathbb{H}_{01} \sigma_3 g_R^a \mathbb{H}_{10}. \quad (20)$$

The linewidth function of the right lead is defined as

$$\Gamma_R = \text{i}(\Sigma_R^r - \Sigma_R^a) = \text{i}(\mathbb{H}_{01} g_R^r \sigma_3 \mathbb{H}_{10} - \mathbb{H}_{01} \sigma_3 g_R^a \mathbb{H}_{10}). \quad (21)$$

For the left leads, the self-energy reads

$$\Sigma_L^r = \mathbb{H}_{10} g_L^r \sigma_3 \mathbb{H}_{01}, \quad (22)$$

and the corresponding left linewidth function can be calculated as

$$\Gamma_L = \text{i}(\Sigma_L^r - \Sigma_L^a) = \text{i}(\mathbb{H}_{10} g_L^r \sigma_3 \mathbb{H}_{01} - \mathbb{H}_{10} \sigma_3 g_L^a \mathbb{H}_{01}). \quad (23)$$

To distinguish the left- and right-propagating magnon states, we need to calculate the group velocity of magnons at the  $n$ th eigenstate:

$$v_n = \frac{d\omega_n}{dk} = \pm \text{i} u_n^\dagger (\lambda_n \mathbb{H}_{01} - \lambda_n^* \mathbb{H}_{10}) u_n, \quad (24)$$

where the  $\pm$  is dependent of the type of the particles. It can be easily verified that the propagating states and the linewidth function satisfy the relation

$$u_n^\dagger \Gamma_R u_{n'} = |v_n| \delta_{nn'}. \quad (25)$$

A similar expression for the left linewidth function also exists. To proceed, we write the right-surface Green's function in terms of eigenvectors  $\{u_n\}$  as

$$g_R^r \sigma_3 \mathbb{H}_{10} = \mathcal{U} \Lambda \mathcal{U}^{-1} = \sum_n u_n \lambda_n \tilde{u}_n^\dagger, \quad (26)$$

where  $\tilde{u}_n$  and  $\tilde{u}_n^\dagger$  are the  $n$ th column and row of  $\mathcal{U}^{-1}$ , respectively. The linewidth function can be further written as

$$\begin{aligned} \Gamma_R &= \text{i}(\mathbb{H}_{01} g_R^r \sigma_3 \mathbb{H}_{10} - \mathbb{H}_{01} \sigma_3 g_R^a \mathbb{H}_{10}) \\ &= \text{i} \sum_{n,m} \tilde{u}_m (u_m^\dagger \mathbb{H}_{01} u_n \lambda_n - \lambda_m^* u_m^\dagger \mathbb{H}_{10} u_n) \tilde{u}_n^\dagger \\ &= \sum_n \tilde{u}_n |v_n| \tilde{u}_n^\dagger, \end{aligned} \quad (27)$$

where we have used Eq. (24) and inserted the unitary matrix  $\mathbb{1} = \sum_m u_m \tilde{u}_m^\dagger = \sum_m \tilde{u}_m u_m^\dagger$ . We obtain the relation of the linewidth function for later usage:

$$\Gamma_{L/R} = \sum_n \frac{1}{|v_n|} \Gamma_{L/R} u_n u_n^\dagger \Gamma_{L/R}. \quad (28)$$

Using  $\mathcal{G}^r(\omega - \sigma_3 \mathbb{H}) = \mathbb{1}$  and the Schrödinger equation  $(\omega - \sigma_3 \mathbb{H}) \Psi_n^{(\ell)} = 0$  for the  $n$ th asymptotic scattering state in the lead  $\ell$ , we can write the wave function in real space as

$$\begin{aligned} \Psi_n^{(\ell)}(\mathbf{r}) &= \langle \mathbf{r} | \mathcal{G}^r(\omega - \sigma_3 \mathbb{H}_{\text{spw}}) | \Psi_n^{(\ell)} \rangle \\ &= \sum_j \langle \mathbf{r} | \mathcal{G}^r | j \rangle \langle j | \sigma_3 \mathbb{H}_{\text{spw}} | \Psi_n^{(\ell)} \rangle \\ &\quad - \langle \mathbf{r} | \mathcal{G}^r \sigma_3 \mathbb{H}_{\text{spw}} | j \rangle \langle j | \Psi_n^{(\ell)} \rangle, \end{aligned} \quad (29)$$

where the summation runs over the scattering region and leads. By substituting the Hamiltonian Eq. (11) into Eq. (29), we find that the terms in the scattering region cancel each other and the asymptotic wave function can be reduced into the summation involving only contributions from the surfaces of the leads. Consider the asymptotic wave function in the left lead,

$$\begin{aligned} \Psi_n^{(\ell)}(\mathbf{r}) &= \langle \mathbf{r} | \mathcal{G}^r | x_L \rangle \sigma_3 \mathbb{H}_{01} \langle x_L - 1 | \Psi_n^{(\ell)} \rangle \\ &\quad - \langle \mathbf{r} | \mathcal{G}^r | x_L - 1 \rangle \sigma_3 \mathbb{H}_{10} \langle x_L | \Psi_n^{(\ell)} \rangle, \end{aligned} \quad (30)$$

where  $x_L$  represents the unit cell in the left lead. As  $x_L$  approaches  $-\infty$ , the scattering function takes the asymptotic form for the  $j$ th unit cell in the lead as

$$\Psi_n^{(\ell)}(j) = \phi_n(j) \lambda_n^j = \frac{1}{\sqrt{|v_n|}} u_n e^{\text{i} k_n j}, \quad (31)$$

where the wave function has been normalized by the corresponding group velocity. Ultimately, the wave function in the left lead where the magnons enter the scattering region is given by [41]

$$\begin{aligned} \Psi_n^{(\ell)}(x) &= \frac{1}{\sqrt{|v_{n,\mathcal{I}}|}} \mathcal{G}_{x,0}^r \sigma_3 (\mathbb{H}_{01} \sigma_3 g_L^{a(\ell)} \mathbb{H}_{10} - \mathbb{H}_{01} g_L^{r(\ell)} \sigma_3 \mathbb{H}_{10}) \phi_{n,\mathcal{I}}^{(\ell)} \\ &= \frac{\text{i}}{\sqrt{|v_{n,\mathcal{I}}|}} \mathcal{G}_{x,0}^r \sigma_3 \Gamma_\ell \phi_{n,\mathcal{I}}^{(\ell)}, \end{aligned} \quad (32)$$

where we have used Eq. (27) and the property of the Green's functions  $\mathcal{G}_{x,x'}^r = \mathcal{G}_{x,x''}^r (\sigma_3 \mathbb{H}_{01} g_L^r)^{x''-x'}$ .  $\mathcal{G}_{x,0}^r = \langle x | \mathcal{G}^r | 0 \rangle$  stands for the matrix element of the Green's function between unit cell  $x$  in the scattering region and the 0th unit cell which is the first one in the left lead.  $v_{n,\mathcal{I}}$  denotes the group velocity for the  $n$ th incoming mode of the spin wave described by the vector  $\phi_{n,\mathcal{I}}$ . Similarly,  $v_{n,\mathcal{O}}$  denotes the group velocity for the  $n$ th outgoing mode of the spin wave with the wave function  $\phi_{n,\mathcal{O}}$ . In the practical calculations, the incoming and outgoing modes are classified according to the signs of group velocities.

In the asymptotic region where all evanescent states have decayed, a spin wave arising from the incoming state  $\phi_{n,\mathcal{I}}^{(\ell)}$  is scattered into the outgoing state  $\phi_{m,\mathcal{O}}^{(\ell)}$  in the different leads attached to the scattering region, such that

$$\Psi_n^{(\ell)}(j) = \begin{cases} \phi_{n,\mathcal{I}}^{(\ell)}(j) + \sum_m r_{mn} \phi_{m,\mathcal{O}}^{(\ell)}(j), & \text{if } j \text{ in lead } \ell \\ \sum_m t_{mn}^{(\ell'\ell)} \phi_{m,\mathcal{O}}^{(\ell)}, & \text{if } j \text{ in lead } \ell', \end{cases} \quad (33)$$

where  $r_{mn}$  and  $t_{mn}^{(\ell'\ell)}$  are the reflection and transmission amplitudes between the  $m$ th and  $n$ th propagating magnon states. Note that the reflections occur in the same lead, whereas the transmissions occur between two different leads. Utilizing the



orthogonal relation Eqs. (25) and (32), we obtain the reflection amplitude

$$r_{mn} = \frac{1}{\sqrt{|v_m v_n|}} (i\phi_{m,\mathcal{O}}^{(\ell)\dagger} \Gamma_\ell \mathcal{G}_{00}^r \sigma_3 \Gamma_\ell \phi_{n,\mathcal{I}}^{(\ell)} - \phi_{m,\mathcal{O}}^{(\ell)\dagger} \Gamma_\ell \phi_{n,\mathcal{I}}^{(\ell)}), \quad (34)$$

and the transmission amplitude

$$t_{mn}^{(\ell\ell)} = \frac{i}{\sqrt{|v_m v_n|}} \phi_{m,\mathcal{O}}^{(\ell)\dagger} \Gamma_\ell \mathcal{G}_{N+1,0}^r \sigma_3 \Gamma_\ell \phi_{n,\mathcal{I}}^{(\ell)}, \quad (35)$$

where  $\mathcal{G}_{00}^r(\omega) = \langle 0 | \mathcal{G}^r(\omega) | 0 \rangle$  and  $\mathcal{G}_{N+1,0}^r(\omega) = \langle N+1 | \mathcal{G}^r(\omega) | 0 \rangle$  are the matrix elements of the total Green's function, where 0 and  $N+1$  denote the first unit cell of the left and right leads, respectively. Equation (34) and (35) are the generalized Fisher-Lee relations for coherent magnon transport.

### C. Thermal conductance of magnons

In analogy with the phonon transport, the energy flux of magnons through a scattering region connected to two leads at different temperatures  $T_L$  and  $T_R$  is given by [42–44]

$$Q = \int_0^\infty \frac{d\omega}{2\pi} \hbar\omega \mathcal{T}(\omega) [n_B(T_L) - n_B(T_R)], \quad (36)$$

where  $n_B(\omega, T_{L/R}) = \{\exp(\hbar\omega/k_B T_{L/R}) - 1\}^{-1}$  with  $k_B$  being the Boltzmann constant is the Bose-Einstein distribution for magnons, and  $\mathcal{T}(\omega)$  is the magnon transmission coefficient obtained with the help of Eq. (35):

$$\mathcal{T}(\omega) = \sum_{m,n} |t_{mn}(\omega)|^2, \quad (37)$$

where the summations of  $m, n$  run over all propagating states of magnons.

The longitudinal thermal conductance of the wire is defined as  $\kappa_{xx} = Q/\Delta T$ , where  $\Delta T = T_L - T_R$  is the temperature difference between the reservoirs. In the linear response regime, the longitudinal thermal conductance of magnons takes the form

$$\kappa_{xx}(T) = \frac{1}{2\pi} \int_0^\infty \hbar\omega \mathcal{T}(\omega) \frac{\partial n_B(\omega, T)}{\partial T} d\omega, \quad (38)$$

where the partial derivative of the Bose-Einstein distribution  $n_B$  with respect to temperature  $T$  yields

$$\frac{\partial n_B(\omega, T)}{\partial T} = \frac{\hbar\omega}{k_B T^2} e^{\hbar\omega/k_B T} (e^{\hbar\omega/k_B T} - 1)^{-2}, \quad (39)$$

Finally, the longitudinal thermal conductance of two-terminal spin-wave systems is given by

$$\kappa_{xx}(T) = \frac{k_B}{2\pi} \int_0^\infty \mathcal{T}(\omega) \left( \frac{\hbar\omega}{k_B T} \right)^2 \frac{e^{\hbar\omega/k_B T} d\omega}{(e^{\hbar\omega/k_B T} - 1)^2}. \quad (40)$$

## III. RESULTS AND DISCUSSION

We first demonstrate the energy spectra of magnons in  $\text{CrI}_3$  nanowires with two types of edges. Along the transport direction, the arrangement of edged atoms shown in Figs. 1(a) and 1(b) are represented by zigzag and armchair edges, respectively. The dispersion relations of zigzag and armchair nanowires are present in Figs. 2(a) and 2(b), respectively. The overall band structures for both cases exhibit two asymmetric

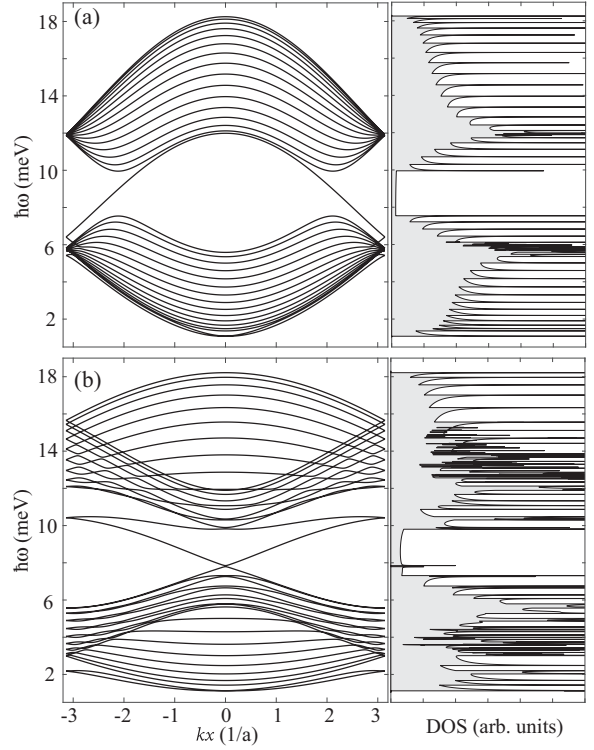


FIG. 2. The dispersion relations (left panel) of Q1D  $\text{CrI}_3$  with zigzag (a) and armchair (b) edges and corresponding density of states (right panels). There are 32 and 40 sites in the zigzag and armchair unit cells, respectively. Here  $J = 0.53$  meV,  $K = 4.07$  meV, and  $A = 0.44$  meV [14].

parts separated by a large bulk gap in which the corresponding DOS are rather small. In contrast with graphene, the edge states in zigzag wires disappear in the present band because the onsite terms in the Hamiltonian depend on the number of neighboring exchange couplings. The states in the bulk gap are chiral and still localized around the edges [14]. The magnon band structure of the armchair wire differs significantly from that of graphene, particularly in the central regime where the chiral states are localized near the boundaries. Moreover, the distinct onsite energies of the edged sites compared with the bulk sites lift the degeneracies of states at specific energies and wave vectors, leading to the anticrossing feature in the armchair band. In the zigzag band, this feature mostly occurs near  $k_x a = \pi$  where bands intersect, making it less pronounced. However, this feature is entirely absent in graphene due to its zero onsite energy. Furthermore, dependent on the width of nanowires, the armchair band structure might possess an intrinsic gap. In the present case as shown in Fig. 2(b), the intrinsic gap is too narrow to be discernible, while the vanishing DOS in the right panel is clearly visible in the vicinity of  $\hbar\omega = 8$  meV.

The DOS are strongly dependent of dimensionality. As shown in the right panels of Fig. 2, the DOS of the zigzag and armchair  $\text{CrI}_3$  nanowires exhibit both one-dimensional (1D) and two-dimensional (2D) characteristics. In 1D systems, the DOS diverge as the inverse of the square root of the energy close to the band extrema, resulting in the prominent “spikes” in the DOS associated with the van Hove singularity. Such

spiky behaviors imply the confinement along the direction perpendicular to the propagating direction of magnons, while the multiple spikes close to onsets of new subbands reflect the extension along the transport direction. Around  $\hbar\omega = 6$  and 12 meV for zigzag wires, numerous band branches aggregate at  $k_x = \pm 3$ , leading to the accumulations of spikes and strong enhancements in DOS. For armchair wires, the enhancements in DOS due to the aggregations of van Hove singularities are preserved but are less pronounced. These features in DOS are in principle observable by spectroscopic experiments [45].

Magnons have potential to implement alternative computing concepts such as nonboolean computing, reversible logic, and artificial neural networks [46]. The logic operators based on the Mach-Zehnder spin-wave interferometer equipped with current-controlled phase shifter can realize the exclusive-not-OR logic gate [47,48]. These applications rely intimately on the coherent propagation of magnons such that theoretical studies of coherent magnon transport in nanodevices are highly relevant. Most prior calculations of coherent transport properties of spin-wave systems have concentrated on pristine systems, while the disorder induced by crystalline imperfections, strain deformations, and magnon-phonon interactions, etc, is inevitable in practical circumstances. The disorder impact on magnon coherent transport and the related thermal properties remains an open issue to explore. Here we simulate two types of disorder: the first one is the exchange randomness by randomly varying the exchanges and the related onsite energy in the magnon Hamiltonian. The strength of disorder is determined by the variations in exchange  $\delta J \in [-\Delta, \Delta]$  in units of  $J$ , namely,  $J_{ij} \rightarrow J + \delta J_{ij}$ . The anisotropic Kitaev term  $K$  is unchanged. Overall, the ratio of  $K/J_{ij}$  remains approximately the same given that the averaged  $\delta J$  is zero. An alternative implementation of disorder in Heisenberg-Kitaev model can also be found in Ref. [49]. The second type of disorder is the spin dilution modeled by removing randomly the spin sites in wires, as illustrated in Fig. 1(c). It has been shown that detailed investigations of disorder effects help clarify the sources of disorder and the nature of the ground state of frustrated spin systems [11,50–52].

In Figs. 3(a) and 3(c), we show the magnon transmission of zigzag and armchair nanowires, respectively, at various concentrations  $p$  of the exchange randomness. The dashed gray lines represent the transmission of the pristine wire for comparison. The finite width of the nanowire quantizes the wave vectors  $k_y$  in the transverse direction giving rise to numerous magnon modes. With the sweep of magnon frequency, these modes are occupied sequentially forming the transmission steps. The variation in strength is fixed to  $\Delta = 0.1$ . The transmission has been averaged over quite a few disorder configurations so that the strong oscillations stemming from scattering are smoothed to some extent. For the zigzag nanowire shown in Fig. 3(a), the transmission steps are smeared by a low disorder concentration, and the quantization feature persists mostly. As the disorder concentration increases, the magnon transmission is suppressed severely with a complete loss of quantization. In the bulk gap regime, the transmission is relatively robust to disorder owing to the absence of backscattering, but sufficiently strong disorder can produce a transport gap analogous to graphene [53]. The fluctuated transmission arises from the scattering by the localized

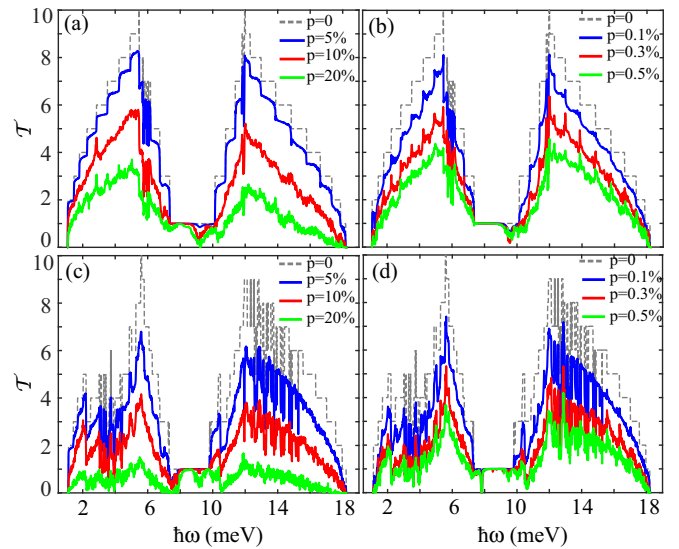


FIG. 3. The magnon transmission of (a), (b) zigzag and (c), (d) armchair nanowires as a function of the magnon energy for different types of disorder. There are 20 and 40 sites in the zigzag and armchair unit cells, respectively. In panels (a) and (c), the nanowires are subject to the exchange randomness, while panels (b) and (d) are subject to spin dilution.  $p$  denotes the concentrations of disordered spin sites.  $\Delta$  accounts for the exchange variation between the nearest-neighbor spins in units of  $J$ . In this case  $\Delta = 0.1$ . The dashed gray lines stand for the propagating modes of the pristine system.

magnon states generated by disorder, which reduces the mean-free path of magnons.

The transmission quantization of armchair wires is more complicated and more sensitive to disorder as shown in Fig. 3(b). Disorder with a low concentration sufficiently restrains the quantized steps in transmission accompanied by sudden drops with the sweep of the magnon energy conforming to the van Hove singularity in DOS. As  $p$  increases, the magnon transmission diminishes dramatically, and exhibits two peaks around  $\hbar\omega = 6$  and 12 meV where the van Hove singularities aggregate resembling those in the zigzag cases. For larger systems whose sizes are much larger than the coherent length, the disorder average should be conducted by summing over all the phase-independent coherent subsystems. In view of the random distribution of disorder, the average is equivalent to an average over the positions of disorder within a single subsystem. In our case, the prominent oscillations will be suppressed after averaging sufficient disorder configurations. Moreover, when the strength of disorder is varied with a fixed  $p$ , the transmission exhibits similar features, namely, the transmission declines as the strength of disorder increases.

Figures 3(b) and 3(d) display the transmission of zigzag and armchair wires, respectively, in presence of the spin dilution. Compared with the case of the exchange randomness, a very small concentration of the spin dilution can destroy the transmission steps in the bulk transport regime and gives rise to strong oscillations, whereas the transmission is relatively robust in the bulk gap regime since the role of the spin dilution amounts to elongating the edges. In principle, the above effects of propagating magnons can be detected

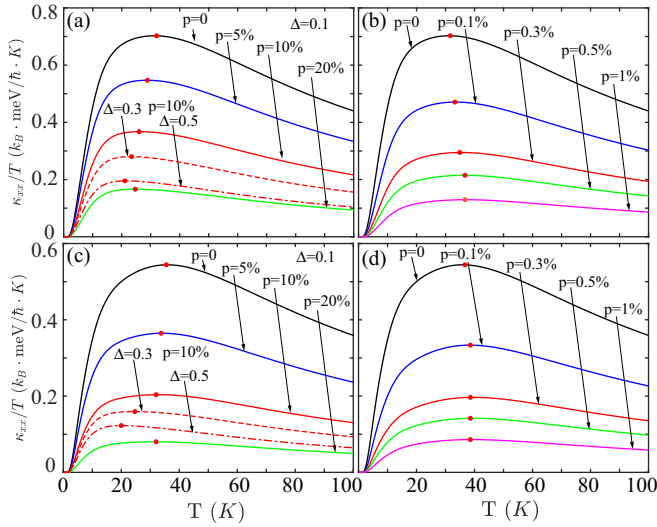


FIG. 4. Temperature  $T$  dependencies of thermal conductance divided by  $T$  for (a), (b) zigzag and (c), (d) armchair nanowires in the presence of (a), (c) the exchange randomness and (b), (d) spin dilution. The unit cells of the zigzag and armchair nanowires contain 80 and 136 sites, respectively.  $p$  denotes the concentrations of disorder.  $\Delta$  denotes the strength of the exchange randomness in units of  $J$ . The positions of the broad peaks are highlighted by red dots.

experimentally by combining the spin-pumping and inverse spin Hall effects [54].

We now proceed to the thermal properties of  $\text{CrI}_3$  by focusing on the longitudinal thermal conductance  $\kappa_{xx}$  since it may provide crucial information of the ground states of Heisenberg-Kitaev magnets. We find that  $\kappa_{xx}$  for all cases undergoes a steep increase at low temperatures as the magnon modes are getting occupied until it approaches a saturated value at higher temperatures (not shown here). In view of that  $\kappa_{xx}$  divided by temperature ( $T$ ) is loosely related to the entropy of the system, we show the temperature dependencies of  $\kappa_{xx}/T$  in Fig. 4 for zigzag and armchair wires with the exchange randomness and spin dilution. In metallic ferromagnets, the adoption of  $\kappa_{xx}/T$  also facilitates the discussion of the Wiedemann-Franz law [34]. The zigzag and armchair wires have nearly the same width for comparison, and the temperature is up to 100 K albeit the Curie temperature is 45 K for ferromagnetic  $\text{CrI}_3$ . Near or above the Curie temperature, thermal spin fluctuations begin to dominate and drive the system into a paramagnetic state. Consequently, the thermopower generated by magnons is expected to decrease significantly. However, experiments and theories have revealed that the short-lived, short-range, locally ordered structures called paramagnons can develop in paramagnets, mitigating the expected thermopower reduction [55]. Nevertheless, the most interesting features that occur in the ferromagnetic phase are of interest to us such that the higher-order magnon-magnon interactions are not very relevant for the present study and the linear-spin-wave scenario is sufficient.

In the ferromagnetic phase,  $\kappa_{xx}/T$  of pristine zigzag and armchair nanowires increases gradually as temperature decreases and then drops dramatically at low temperatures, producing a broad peak around the characteristic temperature

$T_p$ . It tends to zero at high temperatures where all bands are equally occupied, and no bands are occupied at very low temperatures. The similar behaviors of longitudinal and transverse thermal conductivity have been discussed in the Kitaev model based on the theory of quantum spin liquids, in which the peculiar temperature dependence of  $\kappa_{xx}$  is used to probe the fractional quasiparticles inherent to the Kitaev quantum spin liquids [11,12,34]. The Kitaev quantum spin liquid depicts the fractionalization of quantum spin: itinerant Majorana fermions and localized  $Z_2$  fluxes, which well describes properties of materials, such as  $\text{A}_2\text{IrO}_3$  and  $\alpha\text{-RuCl}_3$ . In the present spin-wave scenario, the emergence of the broad peak indicates the growth of the nearest-neighbor (NN) spin correlations along with a release of a significant amount of entropy as suggested by the essence of  $\kappa_{xx}/T$ , in accordance with the role of itinerant Majorana fermions in quantum spin liquids. The peak represents a compromise between the magnon transmission and the mode occupation as encoded in Eq. (40), signifying a maximum entropy release as temperature varies. Our calculations indicate that  $T_p$  is independent of the width of wires.

As disorder is introduced, the suppression of thermal conductance occurs and becomes more prominent with increasing the disorder concentration  $p$  and strength  $\Delta$ , while the broad peak remains intact. In Figs. 4(a) and 4(c), the solid lines represent the thermal conductance with  $\Delta = 0.1$  and  $p$  varying from 0% to 20%. The dashed lines are the cases with the fixed  $p = 10\%$  and  $\Delta$  varying from  $\Delta = 0.3$  to 0.5 for comparison with the red solid line. In Figs. 4(b) and 4(d) corresponding to the cases with the spin dilution, the overall features of thermal conductance are rather similar for both types of disorder, whereas the precise position of peaks evolves differently. For the exchange randomness,  $T_p$  shifts slightly to the low-temperature side, while the peak shifts a bit to the high-temperature side for the spin dilution compared with the pristine case. As the disorder strength increases with a fixed concentration, this feature becomes more evident, as suggested by the dashed lines in Figs. 4(a) and 4(c). The concentration dependence of  $T_p$  is relatively weak and easily saturates at higher concentrations. Similar behaviors of thermal conductance with respect to disorder were also found in the Kitaev model [11].

The behaviors of peaks described above can be understood as follows:  $T_p$  is associated with the development of the NN spin correlations corresponding to the formation of a kind of “ordering” that leads to a reduction in entropy. For the first type of disorder, random exchanges disturb the states enhancing their degree of uncertainty and leading to an increase in entropy of the system. Therefore, the formation of spin correlations in this case has to be compensated by a lower temperature. For the second type of disorder, some local spins are removed such that the possible states diminish resulting in a lower entropy which is connected to the number of states according to the Boltzmann relation. As a result, the spin correlation for the spin dilution can be developed at higher temperatures compared with the pristine case.

We finally make further remarks on the validity of our model and calculation results. In our calculations, the Curie temperature is not directly involved. However, the values of exchange couplings and anisotropy, derived from

first-principles calculations, can be utilized to predict the critical temperature based on the spin-wave theory. The theoretical estimations of Curie temperature for  $\text{CrI}_3$  vary from 85 to 33 K depending on the adopted models [26]. The magnetization at low temperatures can be treated within the linear spin-wave framework. At higher temperatures, a reasonable Curie temperature can be estimated by using the nonlinear spin-wave theory with magnon-magnon interactions. Therefore, the Curie temperature within the linear spin-wave framework in our case is expected to be higher than the experimental value 45 K since the strong fluctuations and higher-order terms are not taken into account. Our calculations accurately depict the thermal conductivity with disorder at low temperatures and also provide valuable insights into the overall behaviors of thermal conductivity near the Curie temperature, particularly in the absence of anomalous features. To unravel the anomalous behaviors of thermal conductivity in proximity to the critical point, it is crucial to incorporate nonlinear terms in the Holstein-Primakoff transformation along with the strong fluctuations [56].

#### IV. SUMMARY AND CONCLUSIONS

We have generalized the Fisher-Lee formula and related Green's function theory for the studies of the magnon spectra and thermal properties of spin-wave systems whose Hamiltonian contains the anomalous "particle-hole" interactions after the Holstein-Primakoff transformation. The coherent transport of magnons in the ferromagnet  $\text{CrI}_3$  nanowires in the presence of two types of disorder has been investigated based

on the developed formalism. Both types of disorder strongly modify the magnon transmission and demolish its quantized steps easily. Despite graphene-like edge states are absent, the DOS for zigzag and armchair wires features sharp spike structures as a result of van Hove singularities reflecting the characteristics of Q1D systems. The striking transmission oscillations emerge due to the scattering from magnon localized states and are built up by the van Hove singularity-induced mode jumping. These results are particularly significant for the fabrication of logic gates in magnonics.

Furthermore, we have calculated the longitudinal thermal conductance of two-terminal disordered  $\text{CrI}_3$  nanowires and observed a broad peak in  $\kappa_{xx}/T$  as a signature of the spin-correlations as the temperature decreases. The precise position of peaks shifts slightly with respect to temperature dependent on the type of disorder present. The exchange randomness raises the uncertainty of states and the related entropy, impeding the formation of spin-correlations. Conversely, the spin dilution shrinks the possible states, benefiting the development of spin-correlations to some extent. This behavior of peaks in the spin-wave scenario is reminiscent of that observed in the quantum spin liquid, offering an alternative interpretation of thermal conductance in anisotropic ferromagnets.

#### ACKNOWLEDGMENT

We thank Ye Xiong for illuminating discussion. H.X. acknowledges financial support from Jiangsu Provincial Department of Education through Grant No. 164080H00210.

- 
- [1] X. Zhang, Y. Zhang, S. Okamoto, and D. Xiao, Thermal Hall effect induced by magnon-phonon interactions, *Phys. Rev. Lett.* **123**, 167202 (2019).
  - [2] R. Shindou, R. Matsumoto, S. Murakami, and J. I. Ohe, Topological chiral magnonic edge mode in a magnonic crystal, *Phys. Rev. B* **87**, 174427 (2013).
  - [3] S. A. Owerre, A first theoretical realization of honeycomb topological magnon insulator, *J. Phys.: Condens. Matter* **28**, 386001 (2016).
  - [4] A. Roldán-Molina, A. S. Nunez, and J. Fernández-Rossier, Topological spin waves in the atomic-scale magnetic skyrmion crystal, *New J. Phys.* **18**, 045015 (2016).
  - [5] A. Roldán-Molina, M. J. Santander, A. S. Núñez, and J. Fernández-Rossier, Quantum theory of spin waves in finite chiral spin chains, *Phys. Rev. B* **89**, 054403 (2014).
  - [6] B. Lenk, H. Ulrichs, F. Garbs, and M. Münzenberg, The building blocks of magnonics, *Phys. Rep.* **507**, 107 (2011).
  - [7] R. Matsumoto and S. Murakami, Theoretical prediction of a rotating magnon wave packet in ferromagnets, *Phys. Rev. Lett.* **106**, 197202 (2011).
  - [8] Y. Kajiwara, K. Harii, S. Takahashi, J. Ohe, K. Uchida, M. Mizuguchi, H. Umezawa, H. Kawai, K. Ando, K. Takanashi, S. Maekawa, and E. Saitoh, Transmission of electrical signals by spin-wave interconversion in a magnetic insulator, *Nature (London)* **464**, 262 (2010).
  - [9] N. Li, R. R. Neumann, S. K. Guang, Q. Huang, J. Liu, K. Xia, X. Y. Yue, Y. Sun, Y. Y. Wang, Q. J. Li, Y. Jiang, J. Fang, Z. Jiang, X. Zhao, A. Mook, J. Henk, I. Mertig, H. D. Zhou, and X. F. Sun, Magnon-polaron driven thermal Hall effect in a Heisenberg-Kitaev antiferromagnet, *Phys. Rev. B* **108**, L140402 (2023).
  - [10] R. Matsumoto and S. Murakami, Rotational motion of magnons and the thermal Hall effect, *Phys. Rev. B* **84**, 184406 (2011).
  - [11] J. Nasu and Y. Motome, Thermodynamic and transport properties in disordered Kitaev models, *Phys. Rev. B* **102**, 054437 (2020).
  - [12] J. Nasu, J. Yoshitake, and Y. Motome, Thermal transport in the Kitaev model, *Phys. Rev. Lett.* **119**, 127204 (2017).
  - [13] P. Laurell and G. A. Fiete, Magnon thermal Hall effect in kagome antiferromagnets with Dzyaloshinskii-Moriya interactions, *Phys. Rev. B* **98**, 094419 (2018).
  - [14] E. Aguilera, R. Jaeschke-Ubierno, N. Vidal-Silva, Luis E. F. Foa Torres, and A. S. Nunez, Topological magnonics in the two-dimensional van der Waals magnet  $\text{CrI}_3$ , *Phys. Rev. B* **102**, 024409 (2020).
  - [15] L. Hao, D. Meyers, C. Frederick, G. Fabbris, J. Yang, N. Traynor, L. Horak, D. Kriegner, Y. Choi, J.-W. Kim, D. Haskel, P. J. Ryan, M. P. M. Dean, and J. Liu, Two-dimensional  $J_{\text{eff}} = 1/2$  antiferromagnetic insulator unraveled from interlayer exchange coupling in artificial perovskite iridate superlattices, *Phys. Rev. Lett.* **119**, 027204 (2017).
  - [16] J. Chaloupka, G. Jackeli, and G. Khaliullin, Zigzag magnetic order in the iridium oxide  $\text{Na}_2\text{IrO}_3$ , *Phys. Rev. Lett.* **110**, 097204 (2013).



- [17] K. Foyevtsova, H. O. Jeschke, I. I. Mazin, D. I. Khomskii, and R. Valentí, *Ab initio* analysis of the tight-binding parameters and magnetic interactions in  $\text{Na}_2\text{IrO}_3$ , *Phys. Rev. B* **88**, 035107 (2013).
- [18] A. Koitzsch, C. Habenicht, E. Müller, M. Knupfer, B. Büchner, H. C. Kandpal, J. van den Brink, D. Nowak, A. Isaeva, and T. Doert,  $J_{\text{eff}}$  description of the honeycomb Mott insulator  $\alpha\text{-RuCl}_3$ , *Phys. Rev. Lett.* **117**, 126403 (2016).
- [19] S. M. Winter, Y. Li, H. O. Jeschke, and R. Valentí, Challenges in design of Kitaev materials: Magnetic interactions from competing energy scales, *Phys. Rev. B* **93**, 214431 (2016).
- [20] R. D. Johnson, S. C. Williams, A. A. Haghighirad, J. Singleton, V. Zapf, P. Manuel, I. I. Mazin, Y. Li, H. O. Jeschke, R. Valentí, and R. Coldea, Monoclinic crystal structure of  $\alpha\text{-RuCl}_3$  and the zigzag antiferromagnetic ground state, *Phys. Rev. B* **92**, 235119 (2015).
- [21] C. Gong, L. Li, Z. Li, H. Ji, A. Stern, Y. Xia, T. Cao, W. Bao, C. Wang, Y. Wang, Z. Q. Qiu, R. J. Cava, S. G. Louie, J. Xia, and X. Zhang, Discovery of intrinsic ferromagnetism in two-dimensional van der Waals crystals, *Nature (London)* **546**, 265 (2017).
- [22] B. Huang, G. Clark, E. Navarro-Moratalla, D. R. Klein, R. Cheng, K. L. Seyler, D. Zhong, E. Schmidgall, M. A. McGuire, D. H. Cobden, W. Yao, D. Xiao, P. Jarillo-Herrero, and X. Xu, Layer-dependent ferromagnetism in a van der Waals crystal down to the monolayer limit, *Nature (London)* **546**, 270 (2017).
- [23] B. Huang, G. Clark, D. R. Klein, D. MacNeill, E. Navarro-Moratalla, K. L. Seyler, N. Wilson, M. A. McGuire, D. H. Cobden, D. Xiao, W. Yao, P. Jarillo-Herrero, and X. Xu, Electrical control of 2D magnetism in bilayer  $\text{CrI}_3$ , *Nat. Nanotechnol.* **13**, 544 (2018).
- [24] P. Jiang, L. Li, Z. Liao, Y. X. Zhao, and Z. Zhong, Spin direction-controlled electronic band structure in two-dimensional ferromagnetic  $\text{CrI}_3$ , *Nano Lett.* **18**, 3844 (2018).
- [25] D. Zhong, K. L. Seyler, X. Linpeng, R. Cheng, N. Sivadans, B. Huang, E. Schmidgall, T. Taniguchi, K. Watanabe, M. A. McGuire, W. Yao, D. Xiao, K.-M. C. Fu, and X. Xu, Van der Waals engineering of ferromagnetic semiconductor heterostructures for spin and valleytronics, *Sci. Adv.* **3**, e1603113 (2017).
- [26] J. L. Lado and J. Fernández-Rossier, On the origin of magnetic anisotropy in two dimensional  $\text{CrI}_3$ , *2D Mater.* **4**, 035002 (2017).
- [27] N. D. Mermin and H. Wagner, Absence of ferromagnetism or antiferromagnetism in one- or two-dimensional isotropic Heisenberg models, *Phys. Rev. Lett.* **17**, 1133 (1966).
- [28] A. T. Costa, D. L. R. Santos, N. M. R. Peres, and J. Fernández-Rossier, Topological magnons in  $\text{CrI}_3$  monolayers: An itinerant fermion description, *2D Mater.* **7**, 045031 (2020).
- [29] Y. Onose, T. Ideue, H. Katsura, Y. Shiomi, N. Nagaosa, and Y. Tokura, Observation of the magnon Hall effect, *Science* **329**, 297 (2010).
- [30] H. Katsura, N. Nagaosa, and P. A. Lee, Theory of the thermal Hall effect in quantum magnets, *Phys. Rev. Lett.* **104**, 066403 (2010).
- [31] R. Matsumoto, R. Shindou, and S. Murakami, Thermal Hall effect of magnons in magnets with dipolar interaction, *Phys. Rev. B* **89**, 054420 (2014).
- [32] A. Mook, J. Henk, and I. Mertig, Magnon Hall effect and topology in kagome lattices: A theoretical investigation, *Phys. Rev. B* **89**, 134409 (2014).
- [33] T. Ideue, Y. Onose, H. Katsura, Y. Shiomi, S. Ishiwata, N. Nagaosa, and Y. Tokura, Effect of lattice geometry on magnon Hall effect in ferromagnetic insulators, *Phys. Rev. B* **85**, 134411 (2012).
- [34] R. Samajdar, S. Chatterjee, S. Sachdev, and M. S. Scheurer, Thermal Hall effect in square-lattice spin liquids: A Schwinger boson mean-field study, *Phys. Rev. B* **99**, 165126 (2019).
- [35] D. S. Fisher and P. A. Lee, Relation between conductivity and transmission matrix, *Phys. Rev. B* **23**, 6851(R) (1981).
- [36] T. Holstein and H. Primakoff, Field dependence of the intrinsic domain magnetization of a ferromagnet, *Phys. Rev.* **58**, 1098 (1940).
- [37] M. Pizzochero, R. Yadav, and O. V. Yazyev, Magnetic exchange interactions in monolayer  $\text{CrI}_3$  from many-body wavefunction calculations, *2D Mater.* **7**, 035005 (2020).
- [38] J. Colpa, Diagonalization of the quadratic boson Hamiltonian, *Physica A (Amsterdam, Neth.)* **93**, 327 (1978).
- [39] M.-W. Xiao, Theory of transformation for the diagonalization of quadratic Hamiltonians, *arXiv:0908.0787*.
- [40] E. N. Economou, *Green's Functions in Quantum Physics* (Springer-Verlag, Berlin, 2006).
- [41] M. Wimmer, Ph.D. thesis, University of Regensburg, 2009.
- [42] T. Yamamoto and K. Watanabe, Nonequilibrium Green's function approach to phonon transport in defective carbon nanotubes, *Phys. Rev. Lett.* **96**, 255503 (2006).
- [43] L. G. C. Rego and G. Kirczenow, Quantized thermal conductance of dielectric quantum wires, *Phys. Rev. Lett.* **81**, 232 (1998).
- [44] J.-S. Wang, J. Wang, and J. T. Lü, Quantum thermal transport in nanostructures, *Eur. Phys. J. B* **62**, 381 (2008).
- [45] S. Zaric, G. N. Ostojic, J. Kono, J. Shaver, V. C. Moore, M. S. Strano, R. H. Hauge, R. E. Smalley, and X. Wei, Optical signatures of the Aharonov-Bohm phase in single-walled carbon nanotubes, *Science* **304**, 1129 (2004).
- [46] A. V. Chumak, V. I. Vasyuchka, A. A. Serga, and B. Hillebrands, Magnon spintronics, *Nat. Phys.* **11**, 453 (2015).
- [47] T. Schneider, A. A. Serga, B. Leven, B. Hillebrands, R. L. Stamps, and M. P. Kostylev, Realization of spin-wave logic gates, *Appl. Phys. Lett.* **92**, 022505 (2008).
- [48] M. P. Kostylev, A. A. Serga, T. Schneider, B. Leven, and B. Hillebrands, Spin-wave logical gates, *Appl. Phys. Lett.* **87**, 153501 (2005).
- [49] A. Singhanian, J. van den Brink, and S. Nishimoto, Disorder effects in the Kitaev-Heisenberg model, *Phys. Rev. Res.* **5**, 023009 (2023).
- [50] S. Das Sarma, S. Adam, E. H. Hwang, and E. Rossi, Electronic transport in two-dimensional graphene, *Rev. Mod. Phys.* **83**, 407 (2011).
- [51] N. M. R. Peres, Colloquium: The transport properties of graphene: An introduction, *Rev. Mod. Phys.* **82**, 2673 (2010).
- [52] H. Xu, T. Heinzl, and I. V. Zozoulenko, Conductivity and scattering in graphene bilayers: Numerically exact results versus Boltzmann approach, *Phys. Rev. B* **84**, 115409 (2011).
- [53] C. Wickles and W. Belzig, Effective quantum theories for Bloch dynamics in inhomogeneous systems with nontrivial band structure, *Phys. Rev. B* **88**, 045308 (2013).
- [54] A. V. Chumak, A. A. Serga, M. B. Jungfleisch, R. Neb, D. A. Bozhko, V. S. Tiberkevich, and B. Hillebrands, Direct detection

- of magnon spin transport by the inverse spin Hall effect, [Appl. Phys. Lett.](#) **100**, 082405 (2012).
- [55] Y. Zheng, T. Lu, M. M. H. Polash, M. Rasoulianboroujeni, N. Liu, M. E. Manley, Y. Deng, P. J. Sun, X. L. Chen, R. P. Hermann, D. Vashaee, J. P. Heremans, and H. Zhao, Paramagnon drag in high thermoelectric figure of merit Li-doped MnTe, [Sci. Adv.](#) **5**, eaat9461 (2019).
- [56] G. Laurence and D. Petitgrand, Thermal conductivity and magnon-phonon resonant interaction in antiferromagnetic FeCl<sub>2</sub>, [Phys. Rev. B](#) **8**, 2130 (1973).